ELSEVIER

Polymer 42 (2001) 8225–8233

polymer

www.elsevier.nl/locate/polymer

Homogeneous crystal nucleation in short polyethylenes

H. Kraack[a], E.B. Sirota[b], M. Deutsch[a,*]

[a]*Department of Physics, Bar Ilan University, Ramat Gan 52900, Israel*
[b]*Exxon Mobil Research and Engineering Co., Route 22 E., Annandale, NJ 08801, USA*

Received 10 January 2001; received in revised form 10 April 2001; accepted 25 April 2001

Abstract

The homogeneous nucleation of the solid from the melt is studied in low molecular weight (MW) polyethylene samples with a narrow MW distribution and average carbon numbers in the range $38 \leq n \leq 144$. The measurements employ scanning calorimetry on both emulsified and non-emulsified samples, and low- and high-angle X-ray diffraction. The shortest polyethylenes show undercoolings agreeing well with those of monodisperse *n*-alkanes of similar chain lengths. The longer samples extrapolate smoothly between the undercoolings measured for monodisperse alkanes and high-MW polyethylenes with $n \geq 654$. The results support the earlier conclusions that any transition from a full-molecule nucleation to a 'bundle' nucleation must occur well below $n \approx 25$. The absence of significant features around $n = 120$ where chain folding is expected to set in, implies that it may not occur at the nucleation stage, or may have no significant contribution to the nucleation energetics. © 2001 Elsevier Science Ltd. All rights reserved.

Keywords: Polyethylene; Nucleation; Alkanes

1. Introduction

Normal alkanes, linear chain molecules of the structure $H(CH_2)_nH$, (denoted C_n), are the fundamental building blocks of many organic molecules, and, in particular, of polymers. The nucleation of their crystal phase from the melt attracted much experimental and theoretical attention, ever since the pioneering work of Turnbull and Cormia [1] showed the anomalous behavior of their nucleation for $16 < n < 32$. Their relative undercoolings, $\Delta T/T_m$, where ΔT is the undercooling of the melt below its equilibrium melting temperature T_m, was found in homogeneous nucleation experiments to be ~0.04, fivefold smaller than the ~0.2 found for almost all other organics and almost 10-fold lower than the ~0.3 of metals [2,3]. We have recently shown [4] that the anomalous nucleation behavior is closely related to the existence and phase behavior of the rotator phases, which are among the most characteristic features of normal alkanes. These are plastic crystal phases, of lamellar structure, with long-range translational in-plane order of the molecular center of mass. There is, however, no long-range order in the azimuthal orientation of the molecular plane about the long molecular axis, which is, in general, normal to the lamellar planes [5–12]. The intermediate order of these phases renders their nucleation barrier exceptionally low, thus considerably reducing the undercooling. Recent measurements [13,14] indicate that alkane nucleation may go through a metastable rotator phase even for alkanes not exhibiting a stable equilibrium rotator phase. The anomalously low undercoolings in homogeneous nucleation, and their near absence ($\Delta T \lesssim 0.05$°C) in heterogeneous nucleation in this chain length region are also closely related [4] to another unusual effect observed in these, and related, materials. From general principles, surfaces usually melt at a temperature lower than the bulk, an effect known as surface melting. In normal alkanes, however, the opposite effect, surface freezing, was found to occur [15–23]. Here, the molten bulk coexists with a crystalline surface monolayer up to a few degrees above the bulk freezing temperature T_f for a chain length range which is roughly the same as that showing anomalous nucleation properties.

The undercoolings observed in homogeneous nucleation of alkanes up to $n \approx 30$, $\Delta T \approx 13$°C, are almost independent of n. We have recently extended these measurements up to $n = 60$ and found that at about $n \approx 25$ the undercoolings ΔT start increasing with n, reaching $\Delta T \approx 30$°C for $n = 60$ [4]. Moreover, when plotted against $1/n$, the undercoolings for $30 \lesssim n \leq 60$ extrapolate linearly to the values of $\Delta T \approx 60$°C observed, e.g. in the careful experiments of Ross and Frolen [24], for high-MW polyethylenes, which can be considered to have chain lengths of $n = \infty$. This change in the variation of ΔT with n cannot be attributed

* Corresponding author. Tel.: +972-353-18476; fax: +972-353-53298.
E-mail address: deutsch@mail.biu.ac.il (M. Deutsch).

PII: S0032-3861(01)00308-1

to chain folding [25–32], which sets in at $n \approx 200$. Although folding was found to be inducible under special crystallization conditions for lengths as low as $n = 150$ [25,26] and $n = 120$ [29], this is still much higher than the $n \approx 25$ where the increase in ΔT starts. We have suggested that this increase may be due to the fact that a crossover in the nucleation mode at low n has occurred, from full molecule nuclei to bundle nuclei, where the crystalline nucleus comprises a bundle of chain portions, without regard to their ends. Thus, a portion of a specific chain may be part of the crystalline nucleus, while another portion of the same chain may still be part of the melt. The increase in the undercooling beginning at $n \approx 25$ is then attributed to the surface energy increase when the dangling cilia exceed the persistence length [33].

To better assess the validity of this nucleation mode, to investigate possible crossovers to other nucleation modes, and to shed some light on the possible influence of chain folding on the homogeneous nucleation of alkanes, nucleation studies are required for alkanes of n from 60 to a few hundreds. The range $100 \lesssim n \lesssim 500$ is of particular interest for studying the effect of chain folding [25–32]. Such studies of homogeneous nucleation from the melt are not currently available. In view of the large gap existing for lengths larger than $n = 60$ up to a few hundred carbons, we have undertaken such measurements, the results of which are presented here. Since monodisperse alkanes are not commercially available in this length range, our measurements, using the emulsion method [1,34,35], employ commercially available low-MW polyethylene standards, of relatively narrow MW distributions. The measurements and the results obtained are presented and discussed below. Their implications for the nucleation modes of alkanes and the crossover from alkane to polymer behavior have been discussed elsewhere [33].

2. Nucleation theory

Nucleation theory is discussed in detail in several good review articles [2,3]. We will therefore summarize only the most important aspects of homogeneous nucleation, relevant to our experiments. Molecular fluctuations in the supercooled melt lead to the formation of the critical nucleus. Its size is determined through the competition between surface and bulk energies. The free energy of a larger-than-critical nucleus decreases as the nucleus grows, and thus a macroscopic crystal is created. For a smaller-than-critical nucleus, the free energy is reduced by shrinking and so the nucleus dissolves.

The rate I at which these critical nuclei are formed is $I = K_v \exp(-W^*/k_B T)$. K_v is a constant prefactor, W^* is the free energy per unit volume of the critical nucleus, which depends on the shape and size of the nucleus and is inversely proportional to $(\Delta G_v)^2$. ΔG_v is the difference in the free energy per unit volume between the solid and the liquid phases: $\Delta G_v = \Delta S_{il} \Delta T$, where ΔS_{il} is the entropy of the phase transition, l denoting the liquid and i the specific solid phase into which nucleation occurs. k_B is the Boltzmann constant and T is the temperature. Inserting the energy W^* into the expression for I above and taking the logarithm yields: $\ln I = \ln K_v - D/(T(\Delta T)^2)$, where D includes, through ΔG_v, the surface energy of the nucleus. Thus, the slope D of a plot of $\ln I$ vs. $1/(T\Delta T^2)$ can be used to obtain the solid–liquid interfacial energy σ. For the most commonly used spherical nucleus model this yields: $\sigma^3 = 3k_B D/[16\pi(\Delta S_{il})^2]$. The extraction of σ from the measured melting and freezing temperatures and the undercooling will be further discussed below, and is also discussed in detail in Ref. [4].

3. Experiment

3.1. X-ray measurements

High resolution powder X-ray scattering was performed on ExxonMobil's beamline X10A, NSLS, Brookhaven National Laboratory. A double-bounce Ge(111) monochromator produced a collimated beam with a wavelength of $\lambda = 1.619$ Å. A single bounce flat Ge(111) analyzer provided a resolution of $\Delta q = 0.001$ Å^{-1}. The sample was contained in a 2 mm diameter standard thin-wall ($\sim$0.01 mm) quartz capillary, and the measurements were carried out at room temperature. The temperature variation of the diffraction peaks up to melting was studied with low resolution ($\Delta q = 0.1$ Å^{-1}), using a laboratory-based rotating-anode X-ray source with Cu Kα radiation.

To assess the effect of polydispersity on the diffraction pattern, the lowest MW polyethylene sample (denoted below as PE560) was fractionated by dissolving in heptane to form a dilute ($<1\%$) solution, warming till all was dissolved and then cooling to room temperature and centrifuging. The heptane was removed from both the solid and liquid fraction leaving the '560 soluble' and '560 insoluble' fractions of the PE560 material.

3.2. Calorimetry

3.2.1. The calorimeter

Our calorimeter is described in detail in a previous publication [4]. It consists of (a) an inner copper sample cell, suspended by thin teflon strips inside (b) an aluminum enclosure. The enclosure is situated inside (c) an outer heavy aluminum can, which serves as a passive temperature enclosure. The temperature of the aluminum enclosure (b) is controlled electronically to within 0.02°C by two thin-film heaters, a thermistor and a closed-loop PID controller. A temperature range of $-5 \le T \le 130$°C is accessible, using a temperature-controlled (± 0.1°C) water circulator for coarse temperature setting. Two thermistors are used to measure the temperatures: One is attached to the aluminum enclosure (b), close to one of the heaters and used for

controlling the temperature. The other, measuring the sample's temperature, is imbedded in the bottom of the inner copper cell (a). Relative heat capacities are measured by scanning the temperature of the controlled aluminum cell (b) at a slow constant rate and recording the temperature of the inner copper cell (a). The latent heats obtained here were consistent with independent measurements on the pure materials used in this study.

3.2.2. Sample preparation

Four different low MW polyethylene standards, of relatively narrow MW spread, were measured. They were obtained from Scientific Polymer Products and designated PE560, PE800, PE1150, and PE2150, according to their approximate MW. Their reported number- and molecular weight averaged degrees of polymerization are given in Table 1. These materials were studied by other researchers with regard to their structure using electron diffraction [36], their solution properties [37] and their bulk melting behavior [38]. Our measurements were done on emulsified and non-emulsified samples. The main reason for using the emulsion method is the ability to separate the nucleation from the growth process and to remove macroscopic heterogeneous nucleation sites. Since growth rates are larger than a few cm/min [39], micron-sized droplets can be considered to freeze instantaneously upon nucleation. Thus, the measured heat of transition stems merely from the random nucleation process of single droplets and is hardly influenced by a possibly different growth rate of the nucleus towards a macroscopic crystal. As was shown earlier, non-emulsified alkane [4] and high-MW polyethylene [24] samples show much smaller or no undercooling and nucleate heterogeneously.

The emulsions of the two lower-MW polyethylene samples were prepared similarly to alkane emulsions by mixing ~0.25 g of the polyethylene, 6 g of water, 0.3 g of the non-ionic surfactant Igepal CO-890 and ~2 g of ethyleneglycol as a viscosity-increasing component [4]. The emulsions of the two higher-MW polyethylene standards were prepared according to the procedure of Cormia et al. [34] and Ross and Frolen [24]. The polyethylene was repeatedly melted and recrystallized in nitrobenzene while stirring. The resultant polyethylene microspheres were separated in a centrifuge from the nitrobenzene and then redispersed in Igepal CA-630.

Samples for calorimetry were mixed on a hot plate/magnetic stirrer in a covered glass beaker for about 1 h at temperatures at least 10°C above the melting point of the polyethylene. The samples were then transferred to the preheated copper cell, which was sealed and immediately transferred to the calorimeter, keeping the temperature always above the freezing point of the sample. This procedure allowed us to follow the behavior of the emulsion calorimetrically from its formation through the several heating/cooling cycles measured.

3.2.3. Calorimetric measurement procedures

Several cooling–heating cycles were carried out for each sample, with a cooling rate of 0.2°C/min and a heating rate of 0.1°C/min. These rates were chosen as a compromise between the need to minimize temperature gradients in the cell by lowering the rate [12] and the need to shorten the scan duration by increasing the rate. The shorter duration minimized droplet aggregation during the scan, which was particularly a problem for the longer polyethylene.

The sample was mixed again on the hot plate after the first cooling/heating cycle and the measurements were repeated at least three times for each sample without additional remixing. The variations in the nucleation temperature between repeated measurements were smaller than 1°C.

4. Results and discussion

4.1. General

To compare the results obtained here with previous measurements of nucleation in monodisperse alkanes [4,39–41], an effective 'chain length' has to be defined. As the number averaged, n_n, and weight averaged, n_w, lengths differ rather significantly in our samples, we have chosen to take the average of the two, denoted n_a, as the effective length. Although this choice is arbitrary, the n_a-variation of the various quantities derived here fit in smoothly with the n-variation of the same quantities for monodisperse alkane samples [4,39–41] as shown below. The various n values, as well as the length dispersion n_w/n_n of the samples are listed in Table 1.

We note that no solid–solid transition peaks were found in the thermograms of either the emulsified or the non-emulsified samples. The temperature dependent X-ray measurements below also do not show any solid–solid phase transition. Thus, we conclude that no equilibrium rotator phase exists in our samples, in line with the observation that the equilibrium rotator phase vanishes in monodisperse alkanes at $n \approx 40$ [42]. However, this cannot rule out possible nucleation through a transient, non-equilibrium rotator phase in our samples, as discussed for long monodisperse alkanes [4], and even observed in several cases [43].

We now proceed to present and discuss the results obtained in the X-ray and calorimetry measurements on the non-emulsified and emulsified polyethylene samples.

4.2. X-ray results

The high angle scattering pattern of all the samples were the same. The peak positions were $q = 1.511$ and 1.673 Å^{-1}, corresponding to repeat distances of 4.16 and 3.76 Å. The structure is the orthorhombic lamellar form typical of odd and mixed alkanes, waxes and polyethylenes [44], and these distances correspond to the in-plane, lamella-parallel order. Our low-resolution temperature-dependent scans show that

Table 1
The low molecular weight polyethylene samples studied, and the results obtained. n_n, n_w and n_a denote the number averaged and weight averaged carbon numbers and the average of these two. T_m^{exp} is the range of the measured, and T_m^a is the calculated, melting temperatures. T_b and T_f are the non-emulsified and emulsified sample's freezing temperatures and ΔT is the undercooling. D is the best-fit value of the slope in the correction method, and log K_v is the corresponding prefactor. σ for the correction method is the nucleus' interfacial energy calculated assuming a fixed log $K_v = 36$ m^{-3} s^{-1}, as discussed in the text, and crystal-to-liquid (xl) transitions. The following column contains the surface energy obtained from the full fit method. The last column lists the end surface energy σ_e calculated for a cylindrical model of the nucleus with a constant side surface energy of $\sigma_s = 11.8$ mJ/m^2. A detailed analysis of our data within the cylindrical model is given in Ref. [33]

Effective length				Temperatures					Correction method			Full fit, σ (mJ/m^2)	Cylindrical model, σ_e (MJ/m^2)
n_a	n_w	n_n	n_w/n_n	T_m^{exp} (°C)	T_m^a (°C)	T_b (°C)	T_f (°C)	ΔT (°C)	D (10^6 K^3)	log K_v (m^{-3} s^{-1})	σ (mJ/m^2)		
38.3	39.9	36.7	1.09	71.8–79.6	78.2	79.5	56.2	22.0	6.27	33.8	12.4	12.1	8.5
53.1	57.0	49.2	1.18	87.0–93.6	94.1	92.1	63.8	30.3	9.51	38.9	14.3	14.8	15.5
75.2	82.0	68.4	1.20	105.4–110.0	106.8	107.3	73.2	33.6	15.13	29.0	16.7	15.7	18.5
143.3	153.3	133.3	1.15	119.6–123.0	123.1	117.8	75.5	47.6	26.27	43.9	20.1	21.2	45.6

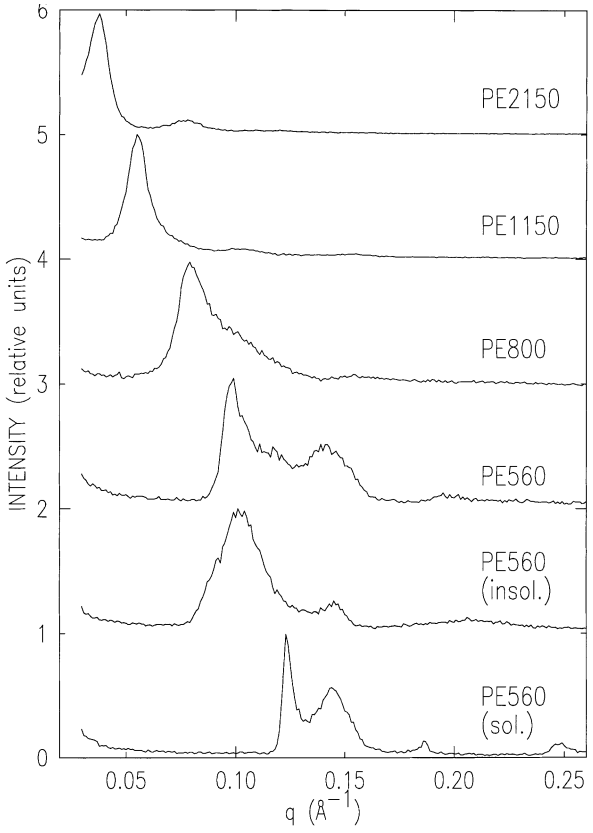

Fig. 1. The low-q region of the X-ray scattering from the samples studied. For a discussion, see text.

this crystalline in-plane structure is maintained as a function of temperature. The only changes observed in the diffraction pattern up to the melting temperature are peak shifts due to thermal expansion. As expected for alkanes of these large chain lengths, no rotator phases were observed prior to melting.

The low-angle scattering from all the samples at room temperature are shown in Fig. 1. These patterns correspond to the lamella-normal order. In all the samples, there is evidence of lamellar stacking, however, the peaks are rather broad. Multiple harmonics can nevertheless be seen: the second in all of the samples and the third in some. The large widths of these peaks are due to the fact that the chain length distribution in these fractions is so broad that not all the chain lengths present in the sample can co-crystallize. Rather, they segregate into crystallites with different compositions. For the case of well-defined single-phase mixtures of alkanes, one can use the 001 peak position to determine the layer repeat distance $d = 2\pi/q$, which can be related to the carbon number $n \approx d/1.27$. When these peaks are broad and in some cases asymmetric or where multiple peaks are observed, the derivation of the structural quantities is not so simple. However, we can use these low-angle peaks to establish some metrics, which relate to the chain length. One way is to use the lowest-q peak's maximum position, q_{peak}. The other is to take a weighted

Table 2
X-ray results for the low molecular weight polyethylene samples. n_a and n_w are the average and weight average carbon number, MW is the molecular weight, q_{peak} and q_{avg} are the lowest-q peak positions, and the weighted q-average over the peak shapes. n_{peak} and n_{avg} are the corresponding X-ray derived carbon numbers

n_a	MW	n_w	q_{avg}	q_{peak}	n_{avg}	n_{peak}
–[a]	560 soluble	39.9	0.137	0.124	36.1	–[b]
–[a]	560 insoluble	39.9	0.108	0.102	45.9	–[b]
38.3	560	39.9	0.119	0.0984	41.6	50.3
53.1	800	57.0	0.0886	0.0790	55.8	62.6
75.2	1150	82.0	0.0530	0.0551	93.3	89.8
143.3	2150	153.3	0.0380	0.0379	130.0[c]	130.0

[a] Distribution not known. n_a cannot be assigned.
[b] Multiple peaks observed.
[c] Probably higher, since the scattering was still significant at lowest q measured.

average of q over the peak shape, q_{avg}. These values and the average carbon number derived from them, n_{peak} and n_{avg}, are shown in the Table 2. Since n_{avg} roughly equals n_a or, at least, it is not a small fraction of n_a, we can safely conclude that chain folding is a negligible factor in determining the lamellar spacing in the length range of our samples.

4.3. Calorimetry results: non-emulsified samples

Typical heating/cooling scans for a non-emulsified $n_a = 75.2$ sample are shown in Fig. 2. These and other non-emulsified samples were measured with a scan rate of 0.1°C/min. In the cooling scans, a relatively sharp peak is observed on freezing at T_b, listed in Table 1. In the heating scans, however, the feature associated with melting is smeared out over a temperature range of 5–15°C and shows no well-defined maximum. Thus, only a range of temperatures, corresponding to points above the peaks' 80% level, are listed as T_m^{exp} in Table 1. The spread renders the determination of T_m from the thermogram highly inaccurate. Consequently, no reliable undercooolings could be derived for the non-emulsified samples. All that can be said from these data is that the undercoolings seem to be small for the shorter samples, while for the longer ones an undercooling of up to a few degrees may exist. For our longest sample, $n_a = 143.3$, an undercooling of 3–4°C seems to be supported by the data. This is in agreement with the increase from zero observed for the undercoolings of non-emulsified monodisperse alkanes around $n \approx 40$, reaching ~0.5°C for $n \approx 60$ [4]. Undercoolings of tens of degrees, such as those observed for emulsified samples of the same materials (see below) can clearly be ruled out for the non-emulsified samples. This is, again, in line with the longest alkane results, where the non-emulsified samples show undercoolings of $\lesssim 0.5$°C while the emulsified ones reach undercoolings of a few tens of degrees [4]. Using temperature modulated differential scanning calorimetry, Pak and Wunderlich [38] obtained recently cleaner data on the bulk supercooling, which are consistent with these results.

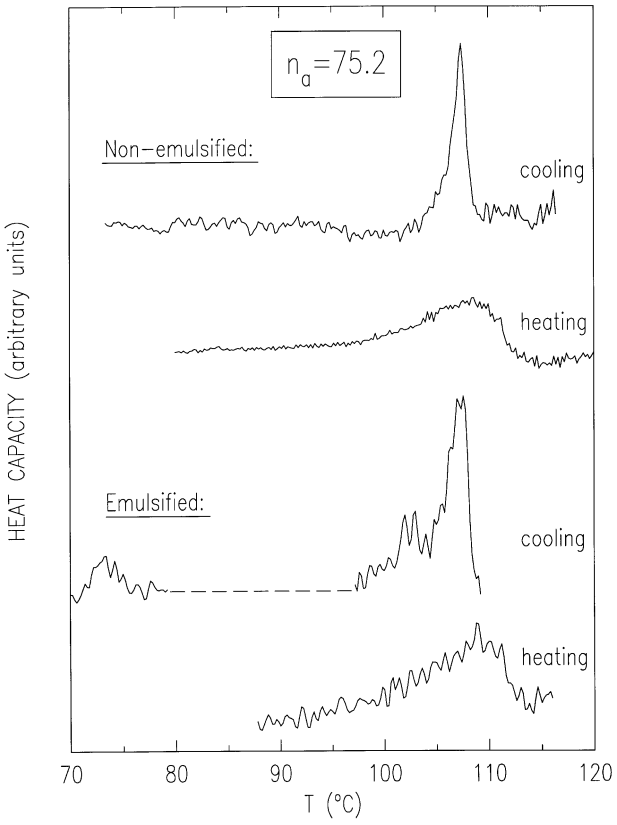

Fig. 2. Cooling and heating thermograms for an emulsified and a non-emulsified polyethylene sample of $n_a = 75.2$. Note the broad melting peaks and the large undercooling in the emulsified sample's cooling scan.

4.4. Calorimetry results: emulsified samples

4.4.1. General features

Fig. 2 also presents cooling and heating thermograms for an emulsified $n_a = 75.2$ sample. The heating scans are practically identical with those of the non-emulsified samples, showing a very broad melting 'peak', which does not allow an accurate determination of an effective melting temperature. We have therefore used the temperatures as calculated for each n_a according to the method of Broadhurst [45]. These are denoted T_m^a and used to calculate the undercoolings $\Delta T = T_m^a - T_f$ where T_f is the measured freezing temperature of the emulsified sample. T_m^a, T_f and ΔT are listed in Table 1.

On the cooling scans (at least) two peaks are observed. The high-temperature peak is due to heterogeneous nucleation of aggregated droplets, a feature observed in all previous measurements on monodisperse alkanes [4,39–41]. The lowest-temperature peak is due to the homogeneous nucleation of the un-aggregated emulsion droplets. As the relative magnitudes of these peaks in Fig. 2 indicate, the high-n_a emulsions are not very stable

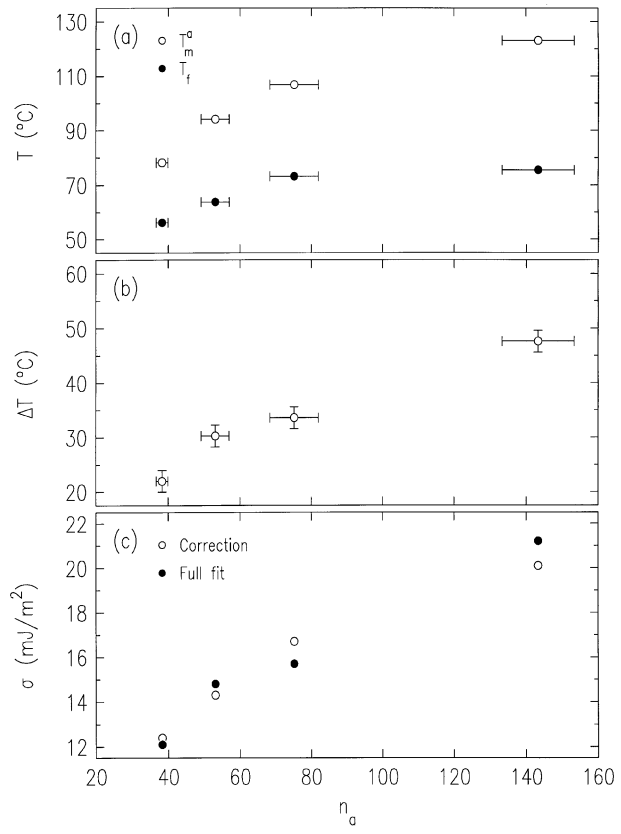

Fig. 3. For the emulsified samples (a) the melting and freezing temperatures, (b) the undercoolings ΔT, and of the surface energies σ derived using the two methods discussed in the text. The x-axis error bars represent the spread in the chain lengths n within the sample, from n_n to n_w. The y-axis error bars represent the measurement errors. The same holds for Figs. 4 and 6.

against aggregation, and only a relatively small part of the emulsion droplets nucleate homogeneously. This is not surprising in view of the polydispersity and lower purity of the present samples, as compared to the alkanes study [4].

The homogeneous nucleation peak was analyzed according to the homogeneous nucleation theory, as detailed below. The small magnitude of the homogeneous nucleation peaks renders the accuracy of derived quantities low. T_f and ΔT, however, could be determined rather accurately, as their variation from scan to scan was <1.5°C. The results derived from the thermograms are listed in Table 1 and plotted in Fig. 3. We now proceed to discuss these results in some detail.

4.4.2. Transition temperatures

The melting, T_m^a, and freezing, T_f, temperatures are plotted in Fig. 3(a). While T_m^a were obtained from Broadhurst's [45] calculations, they compare well with the (admittedly large) measured melting temperature spread T_m^{exp} listed in Table 1. The resultant undercoolings, ΔT, are shown in Fig. 3(b). For the two lowest-MW samples,

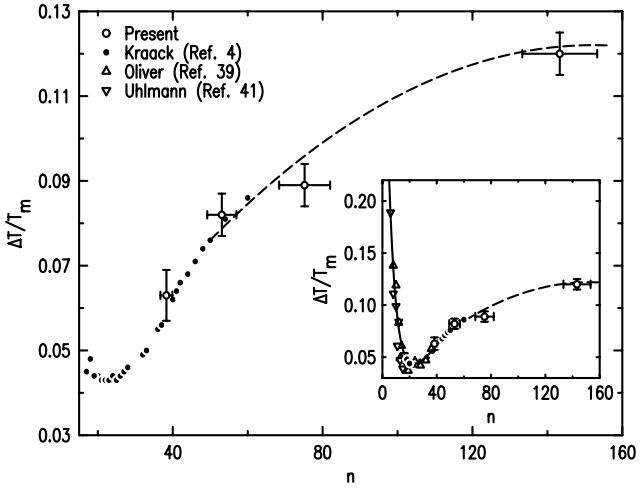

Fig. 4. The relative undercoolings measured (open circles) reported here along with the previous measurements [4] on monodisperse alkanes (closed circles). The inset shows all available relative undercooling data for monodisperse alkanes along with the present results. The lines are just guides to the eye.

where measured data exists for comparable-length monodisperse alkanes [4], both the temperatures and undercoolings agree with the alkane data to within the experimental accuracy. T_m^a and T_f in Fig. 3(a) seem to be reaching saturation for our longest samples, implying near-saturation for the undercooling ΔT as well, as indeed observed in Fig. 3(a). This, in turn, results in the relative undercoolings, $\Delta T/T_m^a$, approaching saturation as well, as shown in Fig. 4. These relative undercoolings agree well with, and continue smoothly the trend set by the monodisperse alkanes. Our largest-n_a sample still does not reach the value of $\sim$0.2 common to organic materials [4], and certainly not the $\sim$0.3 characteristic of almost all other nonmetals [41]. However, it is showing the right trend, and is close to the values of $\sim$0.14 of Ross and Frolen [24] measured for various narrow-distribution polyethylene fractions with $650 \leq n_a \leq 13{,}000$, and to the 0.14–0.2 of Cormia et al. [34], measured for long, practically $n_a = \infty$, polyethylenes.

4.4.3. Interfacial energies

The spherical model [2], which assumes a single surface energy for the critical nucleus, provides a good approximation for metals and other small molecule nucleation, but provides a rather poor approximation for highly anisotropic linear chain molecules such as long n-alkanes [40,41]. In this case, a model with a cylindrical nucleus, having two surface energies, one for the sides and one for the ends of the cylinder, provides a better approximation [4]. Nevertheless, the spherical model is still employed widely [2,34,40,41,46] in interpreting polymer nucleation studies, due to its simplicity and because it allows comparing the resultant 'effective' surface energies with previous studies and other materials. We, therefore, follow here the common

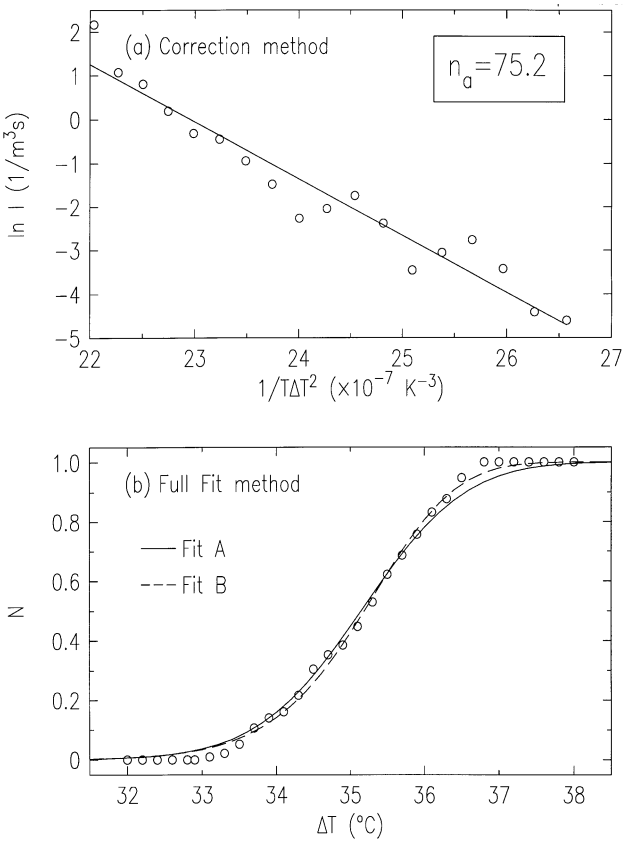

Fig. 5. The fits, discussed in the text, used to extract the interfacial energies σ (a) from the measured relative nucleation rates I, using the correction method and (b) from the measured solid fraction N using the full fit method (b).

practice and provide spherical model surface energies, which should be considered only as effective values. A detailed discussion in terms of a more realistic cylindrical nucleus can be found elsewhere [33].

Two methods were used to extract the surface energy σ and the nucleation prefactor K_v from the measured undercoolings, ΔT,: the correction method [39] and the full fit method [43]. The results obtained by the two methods agree well with each other, lending support to the derived values. We now describe the two methods and discuss the values obtained.

4.4.3.1. The polydispersity correction method. The correction method of Oliver and Calvert [39] employs the nucleation peak lineshape to extract the quantities of physical interest, σ and K_v. The nucleation rate $I(T)$ is calculated first from the measured peak, and corrected for the fact that larger droplets in the droplet size distribution nucleate first. When $I(T)$ is plotted on a semi-logarithmic scale vs. $1/(T\Delta T^2)$, as shown in Fig. 5(a), a linear curve is obtained. For a straight line fitted to these data, the slope determines the interfacial energy σ and the ordinate intersection yields the prefactor K_v. Further details are given in [4].

Because much of the sample nucleates heterogeneously, the homogeneous nucleation peak is rather small and its shape varies from scan to scan. To partly compensate for this variability, a two-step analysis was adopted. First both σ and K_v were obtained as independent variables from the fits. Since K_v is known to be very sensitive to the details of the lineshape [4], our small and rather varied peak shapes resulted in a large variation in the values derived for K_v, as observed in Table 1. Therefore, in the second step of the analysis, the prefactor K_v was fixed for all n_a to the average of the values obtained in the first step: $\log K_v = 36\ \mathrm{m}^{-3}\ \mathrm{s}^{-1}$. The set of surface energies σ obtained from a fit using this fixed K_v is listed in Table 1 under 'correction method'. This $\log K_v$ value, while significantly larger than the $28\ \mathrm{m}^{-3}\ \mathrm{s}^{-1}$ measured by us for the monodisperse alkanes [4], is in very good agreement with the 36 and $37\ \mathrm{m}^{-3}\ \mathrm{s}^{-1}$ values measured by Turnbull and Cormia [1] for $n = 17$ and 18 alkanes, respectively. These isothermal nucleation measurements yield, arguably, the most reliable $\log K_v$ values for short alkanes [4]. The smooth variation obtained for σ with n_a, as observed in Fig. 3(c), and the agreement with higher- and lower-n previous results strongly support this two-step procedure and the values of $\log K_v$ and σ derived from there. The values of σ thus obtained are plotted in Fig. 3(c) and show an approach to saturation akin to, though slower than that observed for the undercoolings in Fig. 3(b).

4.4.3.2. The full curve fit method. Herhold et al. [43] presented recently a novel method for deriving σ and $\log K_v$ directly from the measured solid fraction $N(t)$ vs. time t. For an emulsion with monodisperse droplets of volume V, cooling linearly with time, ($T = T_m - \lambda t$), they obtain:

$$N(\Delta T) = 1 - \exp\left[-AV\sqrt{(D/T_m)}\Gamma\left(-\frac{1}{2}, \frac{D}{T_m(\Delta T)^2}\right)/(2\lambda)\right]. \tag{1}$$

Here Γ is the incomplete Gamma function, $A = K_v/V$, $\Delta T = T_m - T$ is the undercooling, and D includes the surface tension(s) in a model-specific combination. For a spherical nucleus model, the surface tension σ is related to D by $\sigma^3 = 3k_B D/[16\pi(\Delta S_{il})^2]$. In our case, where the sample is polydisperse, an integration over the droplet size distribution $P(V)$ is required. This yields for the average solid fraction $\bar{N}$:

$$\bar{N}(\Delta T) = 1 - \int_0^\infty P(V)\exp\left[-AV\sqrt{(-D/T_m)}\Gamma \times \left(-\frac{1}{2}, \frac{D}{T_m(\Delta T)^2}\right)/(2\lambda)\right]\mathrm{d}V, \tag{2}$$

where $P(V)$ is the log-normal distribution given in [4]. The difference between this method and the polydispersity correction method presented above is that the emulsion

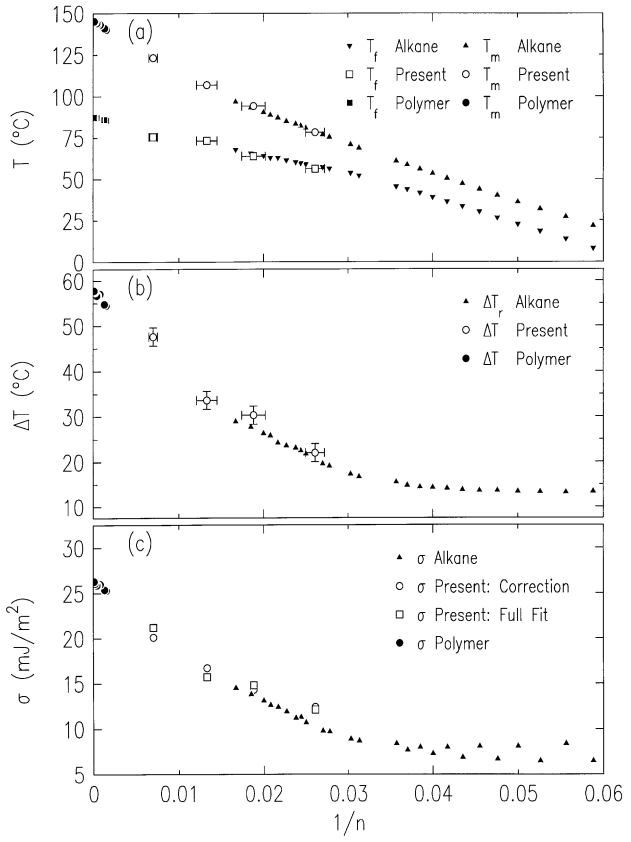

Fig. 6. The melting and freezing temperatures (a), undercoolings (b) and surface energies (c) of emulsified alkanes and high- and low-MW polyethylenes, from the present (open circles) and previous (closed symbols) measurements. For a discussion, see text.

droplets' size distribution is explicitly included. Thus, the approximation of droplet nucleation by strict size order, which must be imposed in the correction method, is not required here. Typical fits to the $n_a = 75.2$ data are shown in Fig. 5(b), for Eq. (1) (Fit A) and Eq. (2) (Fit B). Both employ the same droplet size distribution $P(V)$ measured for monodisperse alkanes and found to be n-independent [4]. As can be observed, both fits are reasonable though Fit B is somewhat better at the higher N values. The slowing down of the nucleation rate as nucleation progresses, observed by Herhold et al. [43], was not found to be necessary in the data fits, and was therefore, not used. The σ values obtained in the two fits are practically identical. They are listed in Table 1 under 'full fit', and plotted in Fig. 3(c).

5. Discussion

Rather well-defined values, listed in Table 1 and plotted in Figs. 3 and 4, emerge from the measurements via the various methods discussed above. The x-axis error bars in that figure were derived from the difference between n_w and n_n. The agreement between results obtained through the correction and the full fit methods for σ lends an increased confidence in the values obtained, in spite of the somewhat arbitrary, though unavoidable, choices made, such as adopting n_a to represent the molecular length and using an average K_v for all n_a. Moreover, our results fit very well into the pattern set by the monodisperse alkanes measurements on the low-n side, and by the high molecular weight polymers on the high-n side of the present n_a range. This can be observed in Fig. 6, which presents plots of the measured T_m, T_f, and ΔT, and the derived σ, vs. $1/n$. The measured values for all the quantities in the figure bridge the gap roughly linearly between the high-MW polyethylene and the low-n monodisperse alkanes. In Fig. 6(a), the melting points, T_m, lie roughly on a straight line over the whole range. However, the freezing points, T_f, show a break around $n \approx 25$ to a lower constant slope for $n > 25$ than that of $n < 25$. This lower slope leads to a significant increase in the undercooling for alkanes with chain lengths longer than $n = 25$ from a constant value of $\Delta T \approx 13$°C for $16 \leq n \leq 28$ up to almost $\Delta T \approx 60$°C for high-MW polyethylenes (Fig. 6(b)). As discussed in more detail elsewhere [33], the break at $1/n \approx 0.04$ ($n \approx 25$) indicates a chain length driven transition between two nucleation modes. For very short alkane molecules, the molecular shape is still not far from spherical, and the nucleation should not differ from that of any other symmetric molecule, i.e. full-molecule nucleation occurs. However, as the molecular length increases (and so does the asymmetry of the alkane molecule) a bundle nucleation should set in, where the nucleus consists of a bundle of chains of nearly full molecules, with protruding cilia, which are smaller than a persistence length. As the molecular length increases, so do the cilia, and a nucleus consisting of a bundle of chains with dangling ends in excess of a persistence length is obtained. As discussed more fully in [33], the break $n \approx 25$ marks the point where the dangling cilia exceed the persistence length, and not the transition (if there is a sharp transition point at all) between full- and partial-molecule nuclei. The smooth behavior derived from our measurements from the highest monodisperse alkane length, $n = 60$, to the high-MW polyethylenes ($n_a > 650$) indicates that whatever mode of nucleation occurs at the highest alkanes ($30 < n < 60$), (whether bundle or other nucleation mode) persists up to high-MW polyethylenes. Chain folding was shown [29] to start appearing during crystal growth for chain lengths not less than $n \approx 120$. The near-equality of n_a and n_{peak} (or n_{avg}), derived from our X-ray measurements and listed in Table 2, clearly indicates that no stable chain-folded phase exists in our sample. The occurrence of a transient chain-folded phase, which converts to a stable non-folded phase is highly unlikely, due to energy considerations. If, however, it does occur, our results indicate that it has no large influence on the macroscopic quantities measured (T_f, T_m) or derived (K_v, σ) here. A better assessment of the role of bundle nucleation and chain folding in the range bridging the gap between high-MW polyethylenes and alkanes will have to await the availability, and careful study, of suitable narrow

length distribution or (preferably) monodisperse alkane/polyethylene samples.

Acknowledgements

An important discussion with Sam Safran (Weizmann Institute) which nucleated this, and a preceding study is gratefully acknowledged. We thank Exxon Research and Engineering Co. for financial support of the work at Bar-Ilan University, NSLS and Exxon for beamtime at and use of X10A, and the MINERVA Foundation for a fellowship to H.K.

References

[1] Turnbull D, Cormia RL. J Chem Phys 1961;34:820.
[2] Kelton KF. Sol Stat Phys 1991;45:75.
[3] Spapen F. Sol Stat Phys 1994;47:1.
[4] Kraack H, Sirota EB, Deutsch M. J Chem Phys 2000;112:15.
[5] Ewen B, Strobl GR, Richter D. Faraday Discuss Chem Soc 1980;69:19.
[6] Doucet J, Denicolo I, Craievich A, Collet A. J Chem Phys 1981;75:5125.
[7] Denicolo I, Doucet J, Craievich AF. J Chem Phys 1983;78:1465.
[8] Ungar G. J Phys Chem 1983;87:689.
[9] Sirota EB, King Jr HE, Singer DM, Shao HH. J Chem Phys 1993;98:5809.
[10] Sirota EB. Langmuir 1997;13:3849.
[11] Sirota EB, Singer DM. J Chem Phys 1994;101:10873.
[12] Sirota EB. Langmuir 1998;14:3133.
[13] Sirota EB, Herhold AB. Science 1999;283:529.
[14] Sirota EB, Herhold AB. Polymer 2000;41:8781.
[15] Wu XZ, Sirota EB, Sinha SK, Ocko BM, Deutsch M. Phys Rev Lett 1993;70:958.
[16] Wu XZ, Ocko BM, Sirota EB, Sinha SK, Deutsch M, Cao BH, Kim MW. Science 1993;261:1018.
[17] Earnshaw JC, Hughes CJ. Phys Rev A 1992;46:R4494.
[18] Hughes CJ, Earnshaw JC. Phys Rev A 1993;47:3485.
[19] Ocko BM, Wu XZ, Sirota EB, Sinha SK, Gang O, Deutsch M. Phys Rev E 1997;55:3164.
[20] Heni M, Lowen H. Phys Rev Lett 2000;85:3668.
[21] Maeda N, Yaminsky VV. Phys Rev Lett 2000;84:698.
[22] Yamamoto Y, Ohara H, Kajikawa K, Ishii H, Ueno N, Seki K, Ouchi Y. Chem Phys Lett 1999;304:231.
[23] Merkl C, Pfohl T, Riegler H. Phys Rev Lett 1997;79:4625.
[24] Ross GS, Frolen LJ. J Res NBS 1975;79A:701.
[25] Ungar G, Stejny J, Keller A, Bidd I, Whitting MC. Science 1985;229:386.
[26] Ungar G, et al. Phys Rev Lett 2000;85:4397.
[27] Hoffman JD, Miller RL. Polymer 1997;38:3151.
[28] Sadler DM. Nature 1987;326:174.
[29] Urabe Y, Tanaka S, Tsuru S, Fujinaga M, Yamamoto H, Takamizawa K. Polym J 1997;29:534.
[30] Teckoe J, Bassett DC. Polymer 2000;41:1953.
[31] Bassett DC, et al. Polymer 1996;37:4993.
[32] Sadler DM. Nature 1987;326:174.
[33] Kraack H, Deutsch M, Sirota EB. Macromolecules 2000;33:6174.
[34] Cormia RL, Price FP, Turnbull D. J Chem Phys 1962;37:1333.
[35] Vonnegut B. J Colloid Sci 1948;3:563.
[36] Dorset DL. Macromolecules 1999;32:162.
[37] Prasad A, Mandelkern I. Macromolecules 1989;22:914.
[38] Pak J, Wunderlich B. J Polym Sci B 2000;38:2810.
[39] Oliver MJ, Calvert PD. J Cryst Growth 1975;30:343.
[40] Calvert PD. J Polym Sci, Polym Phys Ed 1976;14:2211.
[41] Uhlmann DR, Kritchevsky G, Straff R, Scherer G. J Chem Phys 1975;62:12.
[42] Snyder RG, Maroncelli M, Qi SP, Strauss HL. Science 1981;214:188.
[43] Herhold A, Ertas D, Levine AJ, King Jr HE. Phys Rev E 1999;59:6946.
[44] Small M. The physical chemistry of lipids. New York: Plenum Press, 1986.
[45] Broadhurst MG. J Res NBS 1962;66A:241.
[46] Gránásy L, Iglói F. J Chem Phys 1997;107:3634.